A validated model of a photovoltaic water pumping system for off-grid rural communities

Simon Meunier[1*], Matthias Heinrich[2], Loïc Quéval[1], Judith A. Cherni[3], Lionel Vido[4], Arouna Darga[1], Philippe Dessante[1], Bernard Multon[5], Peter K. Kitanidis[6], Claude Marchand[1]

[1]GeePs | Group of electrical engineering - Paris, CNRS, CentraleSupélec, Univ. Paris-Sud, Univ. Paris-Saclay, Sorbonne Univ., Gif-sur-Yvette, France

[2]DargaTech SARL, Ouagadougou, Burkina Faso

[3]Centre for Environmental Policy, Imperial College London, South Kensington Campus, London, UK

[4]SATIE | Systèmes et Applications des Technologies de l'Information et de l'Energie, Univ. de Cergy-Pontoise, Cergy-Pontoise, France

[5]SATIE, ENS Rennes, Univ. de Rennes, CNRS, 35170 Bruz, France

[6]Department of Civil and Environmental Engineering, Stanford Univ., Stanford, CA 94305, United States

[*]Corresponding author. Simon Meunier; E-mail address: simon.meunier@centralesupelec.fr
GeePs, 11 Rue Joliot Curie, 91192 Gif-sur-Yvette, France

Declarations of interest: none

Keywords: Photovoltaic system; Solar resource; Energy conversion; Water pumping; Data validated model

Highlights

- The energy conversion chain in a photovoltaic water pumping system was modelled.
- Water collection by the inhabitants was included as a model input.
- The model was validated by using data acquired on a system in rural Africa.
- The accuracy of the model is higher than 95 % when using local climatic data.
- Accuracy drops of 1 to 3 % when replacing local climatic data by satellite ones.

Abstract
The low electrification rate in rural sub-Saharan Africa prevents access to energy services which are essential to improve living conditions. One of these energy services is electrified water pumping, which is particularly relevant for these areas where water access continues being a significant challenge. Pumping systems powered by photovoltaic energy have emerged as an interesting solution in off-grid areas. This article presents a model of photovoltaic water pumping system (PVWPS) for providing domestic water to off-grid rural communities. The model simulates the pumped flow rate and the water level in the storage tank from the climatic data (irradiance, ambient temperature) and the profile of water collection by the users of the system. The modelling of the different stages of the energy conversion chain and a method for identifying the unknown parameters of PVWPS are presented in this article. The model is applied to a pilot PVWPS situated in a rural village of Burkina Faso. The comparison between the measurements performed on the system and the model outputs allows to validate the model experimentally. Results indicate that the model permits to accurately simulate the water height in the tank both when climatic data from local sensors and from satellite are inputted in the model. The model could therefore be applied to other off-grid areas to perform techno-economic optimization and size new PVWPS as well as to evaluate the performances of existing PVWPS. The originalities of this work include the consideration of the water collection profile as a model input and the monitoring of a PVWPS in a rural village of Sub-Saharan Africa, an area where no continuous measurements on these systems has been performed, to the best knowledge of the authors. Further, the comparison of the impact of inputting satellite climatic data instead of measured ones on the PVWPS model accuracy is also a novel contribution.

Nomenclature

$H_{pa1}(t)$	Additional head due to pressure losses in pipe assembly (PA) 1 (m)
ρ	Albedo of the surrounding environment
$T_a(t)$	Ambient temperature (°C)
$AOI(t)$	Angle of incidence between the sun's rays and the PV modules (rad)
κ_n	Aquifer losses coefficients (s/m^2)
S_t	Area of the base of the tank (m^2)
μ_n	Borehole losses coefficients (s^2/m^5)
β	Coefficient of loss on the maximum power related to modules temperature (°C^{-1})
$I_{pv}(t)$	Current from the PV generator (A)
$G_{dh}(t)$	Diffuse horizontal irradiance (W/m^2)
$G_{dn}(t)$	Direct normal irradiance (W/m^2)
$H_{t,b}$	Height between the ground level and the bottom of the tank (m)
$H_{b,s}$	Height between the ground level and the static water level in the borehole (m)
$H_{b,d}(t)$	Height between the static water level and the water level when there is pumping (drawdown) (m)
η_{stc}	Efficiency of the PV modules in standard test conditions (STC) (%)
$G_{gh}(t)$	Global horizontal irradiance (W/m^2)
$H_{t,i}$	Height between the bottom of the tank and the level at which water enters the tank (m)
$H_{t,r}$	Height between the bottom of the tank and the restart level (m)
$H_{t,s}$	Height between the bottom of the tank and the stop level (m)
$H_t(t)$	Height between the bottom of the tank and the water level in the tank (m)
$G_{pv}(t)$	Irradiance on the plane of the PV modules (W/m^2)
$NOCT$	Nominal operating cell temperature (°C)
ν	Pipe pressure losses coefficient (s^2/m^5)
$P_{pv}(t)$	Power produced by the PV modules (W)
$Q_p(t)$	Pumped flow rate (m^3/s)
$T_{pv}(t)$	PV modules temperature (°C)
θ	Tilt of the PV modules (rad)
t	Time
$TDH(t)$	Total dynamic head (m)
S_{pv}	Total surface covered by the cells of the PV modules (useful surface) (m^2)
$b(t)$	Triggering signal from the controller
$V_{pv}(t)$	Voltage of the PV generator (V)
$Q_c(t)$	Water collection flow rate (m^3/s)

1 Introduction

In 2016, only 25 % of the rural areas of sub-Saharan Africa had access to electricity [1]. As a consequence, many energy services such as lighting, communication, machinery and water pumping cannot be fulfilled. The latter is particularly important because more than 300 million people use unimproved water sources in sub-Saharan Africa, mostly in rural areas [2].

The main energy source for extracting water in these areas is human physical strength, through hand pumps or with buckets in wells [3]. Such collection techniques are time consuming [4], very physically demanding [5] and prevent from reaching deep aquifers [6]. Using electrified solutions from non-renewable or renewable sources has been attempted. In general, these solutions are based on diesel but water pumping systems powered by photovoltaic energy have been expanding. This is notably due to the fact that, thanks to the decreasing costs of photovoltaic (PV) modules [7], these systems have become competitive in off-grid rural areas in terms of life cycle cost [8]. Moreover, they do not emit greenhouse gases at generation point [9], are silent [10], and have low maintenance [11] and operation [12] requirements.

Several models of photovoltaic water pumping systems (PVWPS) have been developed. These models use climatic data as input to simulate the pumped flow rate and focus on different parts of the energy conversion chain. The volume of water pumped for different motor-pump technologies during several months was estimated [13]. Detailed models of the PV array subsystem [14] and the pumping subsystem [14, 15] were presented and their performances for different climatic conditions were simulated. To the best knowledge of the authors, the existing models do not take the water collection profile at the PVWPS as an input. This represents a problem for PVWPS with a specific architecture, which includes a tank and a controller that stops and restarts the motor-pump depending on the water level in the tank. Indeed, the water collection profile influences the water level in the tank and therefore the operation of the motor-pump. As a consequence, without considering the water collection profile, one cannot model correctly PVWPS with this specific architecture, which is nonetheless commonly used for domestic water access.

Several studies have reported experimental measurements on PVWPS in a laboratory environment or for irrigation, in several regions of the world. A laboratory test facility in Algeria was used to validate the models presented in [14] and [15] and experimental data on the operation of PVWPS were collected in laboratories in Greece [16], Tunisia [17] and India [18, 19]. In addition, a PVWPS for irrigation in rural China allowed to validate the models detailed in [20] and [21]. Data on PVWPS for irrigation installed in Egypt [22], Saudi Arabia [23, 24] and Peru [25] were also acquired. Nevertheless, to the best knowledge of the authors, no measurements have been provided on PVWPS for domestic water access in rural villages and none of the studied PVWPS was located in sub-Saharan Africa, despite it being one of the regions with the lowest grid coverage [1] and access to improved water supply [2] and having a high solar energy potential [26]. These elements represent a limitation when it comes to characterising the energetic performances of PVWPS for the particular climate of sub-Saharan Africa and for the particular water use of rural villages.

In addition to previous points, in most articles, the climatic data (irradiance, ambient temperature) used as input of PVWPS models are provided by local measurements. A large number of studies notably use data from weather stations located in North Africa: in different cities of Algeria [14, 27], the southern part of Algeria [28, 29], Tunisia [30] and Egypt [22]. Some other models used local measurements from other parts of the world such as Malaysia [31], China [20, 21], Saudi Arabia [23, 24], Kuwait [32], Greece [33] and India [18, 19]. Fewer models have used climatic data provided by satellite databases. Data from NASA have been utilized for a case study in Ethiopia [34]. Data from Meteonorm have been used for studies in China on irrigation [13, 35] and milk production [36] and for a case study in Morocco [37]. However, to the best knowledge of the authors, the comparison of the impact of inputting satellite data or local measurements on the output of PVWPS models and on their accuracy has not yet been assessed. It is important though to know whether any piece of information may be lost when replacing local sensors for information from satellite.

In this article, a photovoltaic water pumping system model for communal domestic water use in a rural setting is proposed. This model presents the different stages of this energy conversion system that allows the transformation of primary solar resource to an energy service, which is domestic water supply. The model allows to simulate the pumped flow rate and the water level in the tank by using both the water collection profile and climatic data as inputs. The model is validated with data from an installed solar water pumping equipment located in Gogma, a remote village situated in the center-eastern Burkina Faso, Sub-Sahara African. Each day, around 10 m^3 meters are provided by this PVWPS for the domestic water uses of 250 people of the village. To our knowledge, this is the only study that uses experimental data from Sub-Saharan Africa and from a PVWPS for domestic water consumption, allowing a more precise forecast of performance and sustainability of photovoltaic water pumping in this region and for this specific water use. The measurements cover both the dry and the wet season and they are acquired with a time step of ~2.2 s, which permits to grasp the rapid variations of the water use profile. Finally, this study also compares the impact on model output and accuracy of using either climatic satellite data or data from local sensors as input. The model can be applied in other un-electrified villages, to optimize the sizing of new PVWPS and to evaluate the performances of existing PVWPS.

The architecture of PVWPS that is covered by the proposed model and the test site of Gogma are described in section 2; the experimental data collected in Gogma are presented in section 3; the model is detailed in section 4; the validation of the model and the comparison between the use of satellite data and local measurements are presented in section 5.

2 Architecture of the photovoltaic water pumping system considered

The proposed model applies to systems with the architecture presented in Figure 1. The components that are encompassed in this architecture are:

- A PV generator
- A motor-pump with a maximum power point tracking (MPPT) controlled inverter which is immersed in the borehole. The MPPT controlled inverter allows tracking the best operation point of the PV generator. This whole set is called “motor-pump” in the rest of the article.
- A controller which starts and stops the motor-pump according to two set points of the water level in the tank, which is obtained by a float switch.
- A water tank
- A pipe assembly PA1 which links the motor-pump to the tank.
- A fountain at which inhabitants collect water by using taps.
- A pipe assembly PA2 which links the tank to the fountain.

The heights that feature in the model are also presented in Figure 1.

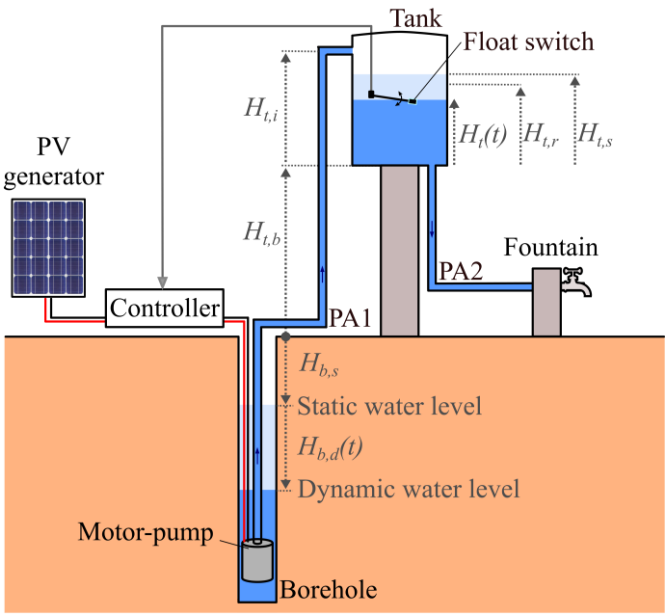

Figure 1 Architecture of the system and definition of the heights
The height datum is set at the ground level so $H_{b,s}$ and $H_{b,d}$ are negative

The PVWPS considered for the case study is in the rural village of Gogma (GPS coordinates: latitude 11.724586; longitude - 0.572290) in the center-eastern Burkina Faso. The system was set up in December 2017 by the company DargaTech, based in Ouagadougou, in collaboration with our research groups. In Gogma the inhabitants mostly work on agriculture for less than 1 $ per day and houses neither have access to electricity nor to piped water. The PVWPS provides water to approximately 250 people each day. They collect the water at the fountain of the PVWPS and use it for 4 types of domestic uses: drinking, cooking, body hygiene and laundry. In general they bring the water back home for drinking, cooking and body hygiene and do the laundry next to the fountain. Figure 2 and Figure 3 show this PVWPS and Table 1 summarizes the parameters of the PVWPS.

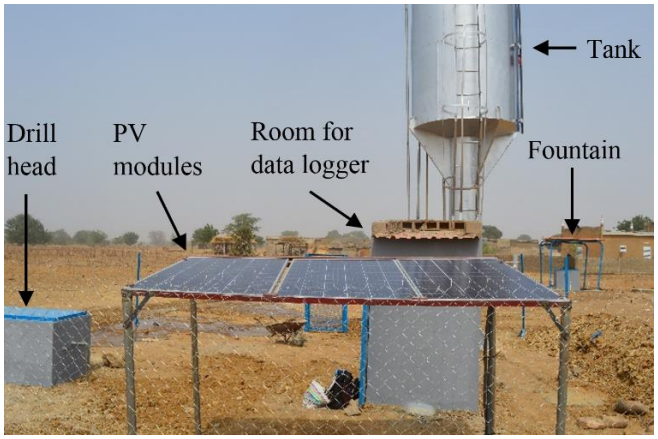

Figure 2 Picture of the PVWPS of Gogma

Figure 3 Overview of the PVWPS
On the left: the fountain where the inhabitants collect water.
On the right: the PV modules and the water tank surrounded by a wire netting

PV generator: 3 multicrystalline silicon modules in series	
Peak power in Standard Test Conditions (STC) according to the datasheet	750 W_p
Total useful surface covered by the cells (S_{pv})	3.9 m^2
Tilt (θ)	0.19 rad (11°)
Azimuth	π rad (180°)
Borehole	
Distance from the ground level to the bottom of the borehole	56 m
Interior diameter of the borehole	0.11 m
Motor-pump: Grundfos SQFlex 5A-7 [38]	
Distance from the ground level to the motor-pump	30 m
Maximum power input	1400 W
Maximum pumping height	50 m
Maximum output flow rate	2.5 10^{-3} m^3/s
Tank: cylindrical made of steel	
Volume	11.4 m^3
Base surface (S_t)	3.3 m^2
Height between the ground level and the bottom of the tank ($H_{t,b}$)	4.2 m
Height between the bottom of the tank and the stop level ($H_{t,s}$)	3.3 m
Height between the bottom of the tank and the restart level ($H_{t,r}$)	3.0 m
Height between the bottom of the tank and the tank input ($H_{t,i}$)	3.4 m
Controller: Grundfos CU 200 [39]	
Pipe assembly PA1: 4 pipes of different diameters and materials	
Total length	47 m
Fountain	
Number of taps	3
Pipe assembly PA2: 1 pipe	
Total length	21 m

Table 1 Parameters of the PVWPS of Gogma

3 Experimental data

In order to identify the unknown parameters of the PVWPS model, to validate it and to monitor the performances of the system installed in Gogma along time, a specific data logger was developed. This data logger was conceived with the idea of minimizing its cost in order to encourage its use for monitoring other PV water pumping installations. The architecture and a picture of the data logger are shown in Figure 4. The data logger is powered by external PV modules (different from the ones of the PVWPS) and the recorded data are collected by using a USB stick. The characteristics of the different sensors are presented in Table 2. In this table, the pumped flow rate Q_p is the flow rate extracted from the borehole and is measured thanks to a flow meter set on PA1. The collected flow rate Q_c corresponds to the water collected by the inhabitants at the fountain. This flow rate is the amount of water retrieved from the water tank and is measured by setting up a flow meter on PA2. From the 14th of January 2018 onward, data have been continuously acquired at Gogma's PVWPS with a

time step of ~2.2 s. The recording rate is equal to the frequency of acquisition. Up to now, more than 200 days of data have been collected which represents more than 5 million points for each of the quantities measured.

Figure 5 presents an example of data collected by the data logger on February 14th, 2018. The sudden interruptions in the pumped flow rate profile correspond to the moments at which the water height in the tank H_t has reached the stop level $H_{t,s}$, which means that the tank is full (at 8h52, 10h06, 12h32 and 13h54 in Figure 5). As the water level in the tank can be directly deduced from the pumped and the collected flow rate, which are both measured, it is also considered as measured. Moreover, in order to avoid a shift of this measured water height in the tank, which may come from the uncertainty on the flow meters measurements, we reset the measured water height to $H_{t,s}$ each time the tank is full.

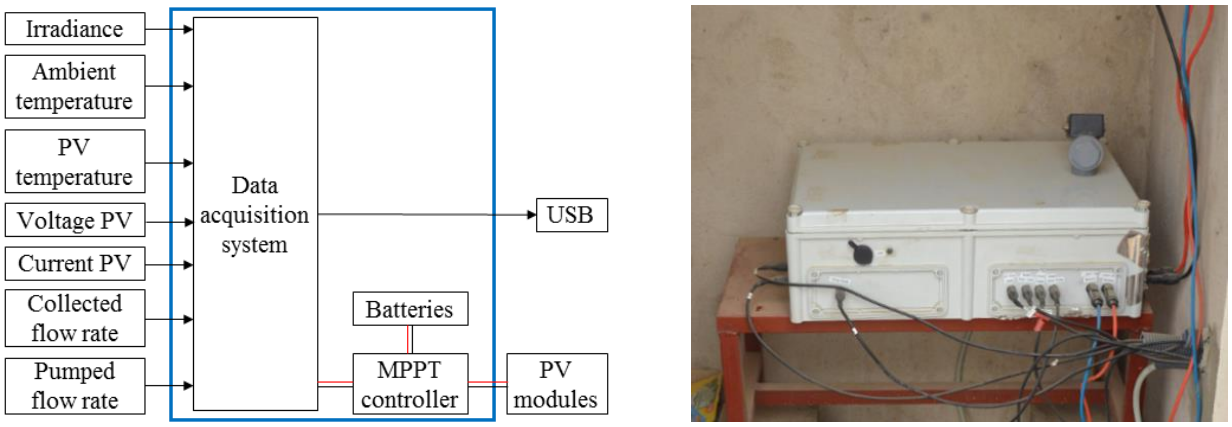

Figure 4 Data logger used for monitoring the PVWPS of Gogma

Measured data	Device	Model	Location	Frequency (Samples/min)	Sensor accuracy
Irradiance on the plane of the PV modules (G_{pv})	Calibrated photovoltaic cell	Solems RG100	On the plane of the PV modules	27	± 10 %
Ambient temperature (T_a)	Platinum resistance thermometer	RS Pro PT1000	In the shadow, next to the PV modules	27	± 0.05 %
PV modules temperature (T_{pv})	Platinum resistance thermometer	RS Pro PT1000	On the back of a PV module	27	± 0.05 %
Voltage of the PV generator (V_{pv})	Voltage transducer	LEM LV 25P	PV generator	27	± 0.9 %
Current from the PV generator (I_{pv})	Current transducer	LEM LA 55P	PV generator	27	± 0.9 %
Pumped flow rate (Q_p)	Turbine flow sensor	HaiHuiLai YF-DN40	On PA1	27	± 5 %
Collected flow rate (Q_c)	Turbine flow sensor	HaiHuiLai YF-DN40	On PA2	27	± 5 %

Table 2 Data monitored by the data logger

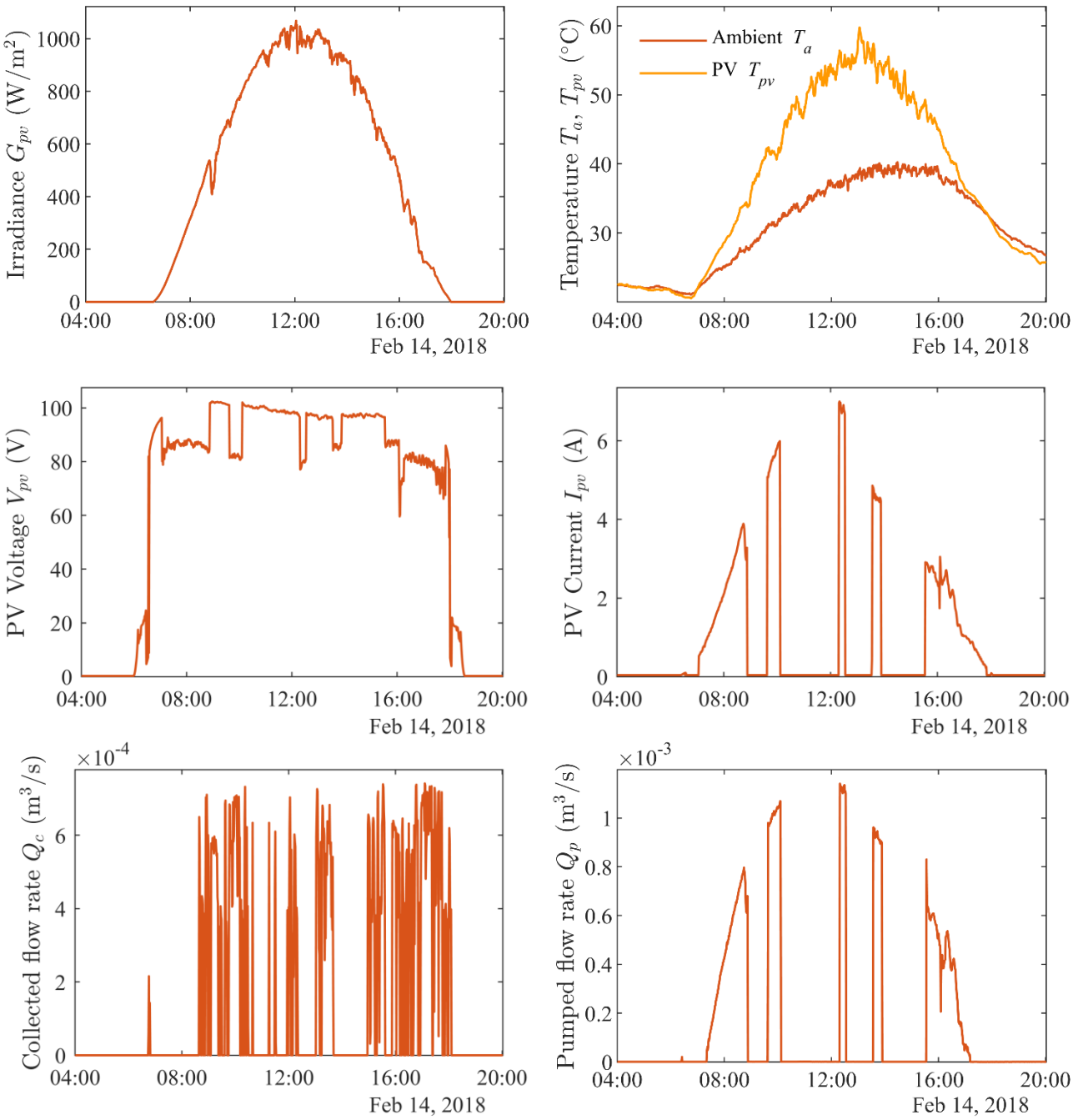

Figure 5 Data collected by the data logger on the 14th of February 2018.

4 Photovoltaic water pumping system model

The proposed model allows to simulate the pumped flow rate and the water level in the tank from climatic and water collection data. The model inputs are the irradiance on the plane of the PV modules G_{pv}, the ambient temperature T_a and the collected flow rate Q_c. The model outputs are the pumped flow rate Q_p and the water level in the tank H_t. The block diagram of the model is presented in Figure 6 and the different submodels are explained in the following subsections.

The application of the model to the PVWPS of Gogma is composed of two phases: identification and validation. The unknown parameters of the system are identified by performing regressions using the measured data from the 12th of February 2018 to the 18th of February 2018 (identification set). The square of the multiple correlation coefficient R^2 is used to estimate the accuracy of identifications. The model validation is then performed by using data from a different period (validation set) and presented in section 5. The model validation will be detailed for the period which last from the 19th of February 2018 to the 21st of February 2018. Moreover, the results of the model validation will also be given for two other validation sets of two weeks. The first one lasts from the 16th of May to the 29th of May 2018 and represents the dry season.

The second one lasts from the 29th of July to the 11th of August 2018 and represents the wet season. The normalized root mean square error $NRMSE$ between the measured and modelled values is used to estimate the accuracy of the model.

For the identification and validation, we used the measured data rescaled to an equally spaced temporal resolution of 1 minute. Indeed, the satellite data that will be used in section 5 are also provided with a time step of 1 minute. We verified by simulation that the results obtained for identification and validation with a time step of 2.2 s were very similar to the ones obtained with a time step of 1 minute.

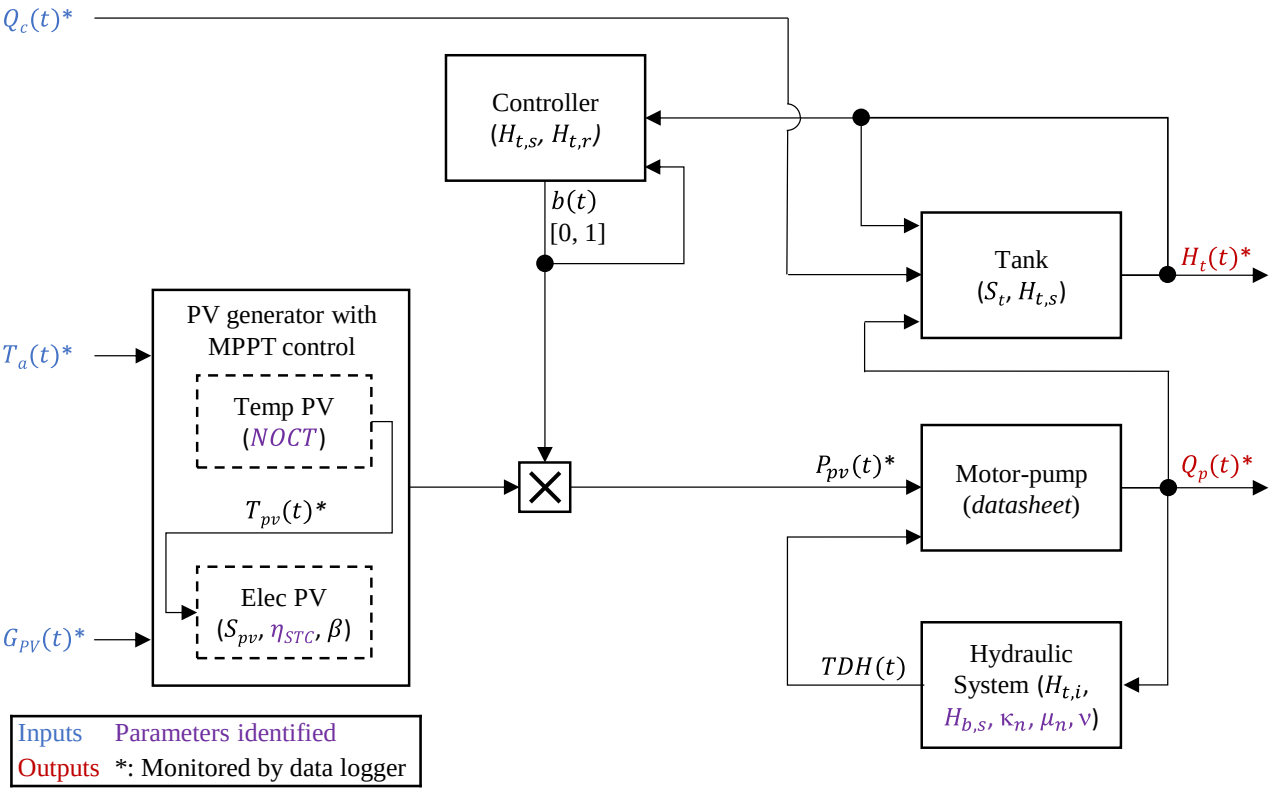

Figure 6 Block diagram of the model.

4.1 Photovoltaic generator

4.1.1 Thermal model

The PV generator thermal model computes the temperature of the PV modules T_{pv} using:

$$T_{pv}(t) = T_a(t) + \frac{NOCT - 20}{800} G_{pv}(t) \quad (1)$$

where T_a is the ambient temperature and G_{pv} is the irradiance on the plane of the PV modules. The $NOCT$ (Nominal Operating Cell Temperature), generally specified by the manufacturer, corresponds to the temperature of the open circuited modules under the following conditions: irradiance on the plane of the modules of 800 W/m^2, ambient temperature of 20°C, wind velocity of 1 m/s and the modules are mounted such that their back side is open.

For the PVWPS of Gogma, the $NOCT$ was not given in the datasheet of the PV modules. The $NOCT$ is therefore determined by identification. To do so, we perform a regression using equation (1) and the experimental data of T_{pv} , T_a and G_{pv} from the identification set. The identification yields to a $NOCT$ of 32 °C ($R^2 = 0.98$). This is low compared to usual values for multicrystalline silicon PV modules, which are in the order of 43 °C to 45 °C [40]. This can be explained by a wind speed higher than 1 m/s and which is not taken into account in the thermal model. Indeed, strong and regular winds have been observed in Gogma and the PV modules are placed at 2 m above ground which favors cooling by convection.

4.1.2 Electrical model

For the PV generator electrical model, considering that the maximum power point tracking of the PV modules is correctly performed by the inverter of the motor-pump, a simplified model is used [41, 42] :

$$P_{pv}(t) = G_{pv}(t)\, S_{pv}\, \eta_{STC} \left(1 + \beta \left(T_{pv}(t) - 25\right)\right) b(t) \quad (2)$$

where P_{pv} is the input power to the motor-pump, S_{pv} is the useful surface of the PV modules, η_{STC} is their efficiency in STC, β is the coefficient of loss on the maximum power related to modules temperature and b is the controller trigger signal (see section 4.2).

For the PVWPS of Gogma, the soiling losses are neglected as the modules are cleaned at least twice a month by the person of the village who is responsible of maintaining the PVWPS. In addition, the PV modules were bought in Burkina Faso and the only documentation that was provided was the tag on the back of the modules. β was not given in the tag and is thus taken equal to - 0.4 %/°C, which is the standard value for multicrystalline silicon modules [41]. According to the tag, the efficiency in STC is equal to 19 %. Nevertheless, since in these regions the tag is not always reliable, it was preferred to determine the value of η_{STC} by identification. A value of 16 % was obtained ($R^2 = 0.96$), which is consistent with the literature [43].

4.2 Controller

The controller is modeled by a switch which transfers ($b = 1$) or not ($b = 0$) the power of the PV modules to the motor-pump depending on the water level in the tank H_t. The value of b is governed by the hysteresis function presented in Figure 7, where $H_{t,s}$ is the water level in the tank for which the motor-pump stops (the tank is full) and $H_{t,r}$ is the level for which it restarts.

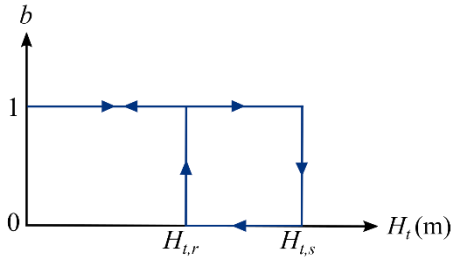

Figure 7 Controller model.

For the PVWPS of Gogma, the ratio $\frac{H_{t,s}-H_{t,r}}{H_{t,s}}$ is equal to 9 %.

4.3 Tank

As the tank is sealed, it is considered that no water leaves the tank by evaporation. The height of water in the tank H_t is expressed as:

$$H_t(t_0) = H_{t,s}$$
$$H_t(t) = H_t(t_0) + \int_{t_0}^{t} \frac{Q_p(\tau) - Q_c(\tau)}{S_t} d\tau \quad (3)$$

where Q_p is the pumped flow rate, Q_c is the water collection flow rate and S_t is the area of the base of the cylindrical tank. The model is initialized at a time t_0 at which the water level has just reached the stop level $H_{t,s}$, the motor-pump has just stopped pumping and b has just switched from 1 to 0. This time t_0 is identified by finding an interruption in the pumped flow rate profile. Once it has been identified, only climatic data and water collection data are required for running the whole model.

4.4 Motor-pump

The characteristic of the motor-pump provided by the manufacturer is used to build the motor-pump model. This characteristic links the total dynamic head TDH, the pumped flow rate Q_p and the input power P_{pv}. The points of the characteristic for which $Q_p > 0$ are fitted by a 4th order polynomial $P_a^{4,4}$. This provides a precise approximation while maintaining a low computing time. The pumped flow rate is thus given by:

$$Q_p(t) = \max\left(0,\ P_a^{4,4}\left(P_{pv}(t), TDH(t)\right)\right) \quad (4)$$

For the PVWPS of Gogma, the fitting is very accurate (R^2 = 1.00) and the coefficients of the polynomial are presented in appendix in section 7. Figure 8 presents the points from the datasheet and the surface obtained by fitting (corresponding to equation (4)).

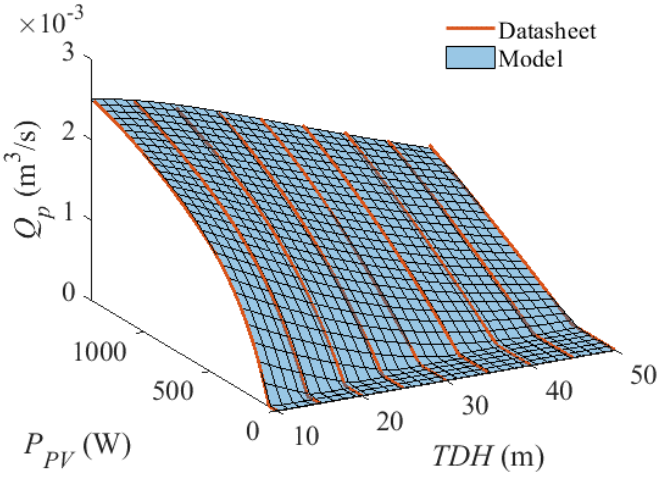

Figure 8 Characteristic surface of the motor-pump SQFlex 5A-7

4.5 Hydraulic system

The total dynamic head TDH between the motor-pump and the tank is given by:

$$TDH(t) = -(H_{b,s} + H_{b,d}(t)) + H_{t,b} + H_{t,i} + H_{pa1}(t), \quad \forall P_{pv} \tag{5}$$

where $H_{b,s}$ is the static water level (height between the ground level and the water level in the borehole when there is no pumping; $H_{b,s}<0$), $H_{b,d}$ is the drawdown (height between the static water level and the water level in the borehole when there is pumping; $H_{b,d}<0$), $H_{t,b}$ is the height between the ground level and the bottom of the tank, $H_{t,i}$ is the height between the bottom of the tank and the tank input (independent of the water level in the tank) and H_{pa1} is the additional head due to pressure losses in pipe assembly 1 (Figure 1). $H_{b,d}$ and H_{pa1} can be expressed as function of Q_p only (see sections 4.5.1 and 4.5.2) and equation (5) holds for any value of P_{pv}. This equation therefore represents the equation of a surface versus variables Q_p and P_{pv}, which is called the hydraulic system surface.

4.5.1 Drawdown model

It is considered that the drawdown $H_{b,d}$ changes linearly and quadratically with the pumped flow rate [44] and that the drawdown at a time t also depends on the flow rates at previous times [45]. This drawdown is therefore given by:

$$H_{b,d}(t) = -\sum_{n=0}^{N} \kappa_n Q_p(t - n\,\Delta T) - \sum_{n=0}^{N} \mu_n Q_p(t - n\,\Delta T)^2 \tag{6}$$

where κ_n are coefficients that represent aquifer losses, μ_n represent borehole losses and ΔT is a time difference. The values chosen for N and ΔT depend on the data availability, the accuracy required for the model and the speed of the drawdown response.

For the PVWPS of Gogma, κ_n and μ_n were identified from the step drawdown tests that were performed before the installation of the PVWPS, at the moment of the borehole drilling in November 2017. 4 step drawdown tests were performed for 4 different flow rates ranging from 2.8 10^{-4} m^3/s to 1.8 10^{-3} m^3/s. For each step drawdown test, $H_{b,d}$ was monitored, with a time step of 10 minutes, during one hour of pumping at a given flow rate and during an additional hour when there was no pumping (recovery phase). Regressions of $H_{b,d}$ against Q_p and t with a ΔT of 10 minutes for different values of N were tried. In the end, a model with only κ_0 and μ_0 was selected. Indeed the aquifer response is fast and the statistical significance of the following coefficients ($\kappa_1, \mu_1, \kappa_2, \mu_2 \ldots$) is low. The values obtained for $\kappa_0$and μ_0 are:

$$\kappa_0 = 2.0\ 10^3\ m^{-2}\ s; \mu_0 = 5.8\ 10^5\ m^{-5}\ s^2\ (R^2 = 0.97)$$

Figure 9 presents the drawdown measured during the 4 step pumping tests (at 2.8 10^{-4}, 8.3 10^{-4}, 1.7 10^{-3} and 1.8 10^{-3} m^3/s) and the drawdown simulated by the model. The difference between the model and the pumping test data shows the difficulty of setting up the drawdown model, but the accuracy reached is sufficient for the purposes of this particular PVWPS model (see section 5).

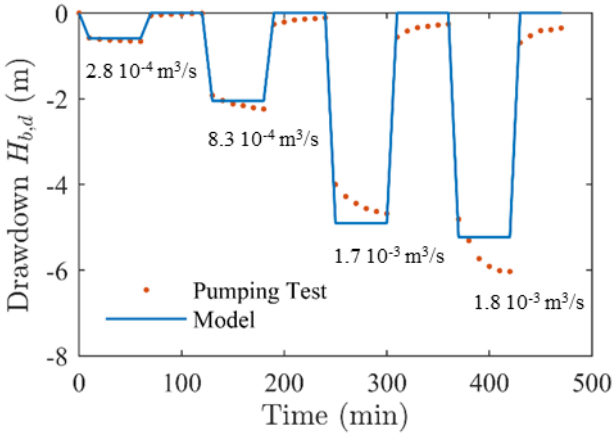

Figure 9 Drawdown measured during the pumping tests and simulated by the model

4.5.2 Pipe model

The additional head due to losses in pipe assembly 1 H_{pa1} evolves quadratically with the flow rate [46]:

$$H_{pa1}(t) = \nu Q_p(t)^2 \tag{7}$$

where ν is a constant. These losses occur along the length of the pipes and at junctions (elbows, curvatures, diameter changes between pipes and pipe output) [46].

In the case of Gogma, ν and $H_{b,s}$ are determined by identification by using equation (5) and (7) and data from the PVWPS operation. As TDH is not measured directly, it is obtained from P_{pv} and Q_p by fitting the motor-pump characteristic with another 4th order polynomial $P_b^{4,4}$ (see appendix in section 7 for the values of the coefficients):

$$TDH(t) = P_b^{4,4}\left(P_{pv}(t), Q_p(t)\right), \forall Q_p > 0 \quad (R^2 = 1.00) \tag{8}$$

By combining equation (5) and (8), all the operating points of the PVWPS, which correspond to the intersection of the motor-pump surface and of the hydraulic system surface, can be found:

$$P_b^{4,4}\left(P_{pv}(t), Q_p(t)\right) = -\left(H_{b,s} - \kappa_0 Q_p(t) - \mu_0 Q_p(t)^2\right) + H_{t,b} + H_{t,i} + \nu Q_p(t)^2 \tag{9}$$

The values of $H_{b,s}$ and ν are identified by using the measured P_{pv} and Q_p from the identification set:

$$H_{b,s} = -4.9 \text{ m}; \nu = 4.9\ 10^6\ m^{-5}\ s^2\ (R^2 = 0.84)$$

The value of the static water level identified is close to the one measured during the step drawdown tests which is of - 6.1 m. The difference may be due to measurement error, seasonal change, model inaccuracy or a combination of these factors. The value of ν is greater than usual values for this type of system, which corresponds to significant head losses due to the pipe assembly 1 (PA1) [46].

For installations for which pumping tests are not available, it is possible to determine the coefficients $(\kappa_n, \mu_n, H_{b,s}, \nu)$ from the intersection of the motor-pump surface and the hydraulic system surface only (equation (9) for the PVWPS of Gogma). However, as μ_0 and ν are both coefficients for $Q_p(t)^2$, only the sum of μ_0 and ν is obtained and not the individual values of the coefficients. This prevents to separate the contributions of the drawdown and the pipe losses to the total dynamic head. It would therefore not be possible to know if the drawdown goes below the level of the motor-pump.

5 Model validation for two types of climatic data

The model inputs are the climatic data (irradiance and temperature) and the collected flow rate. The model outputs are the pumped flow rate and the water level in the tank. To validate the model, the model outputs are compared to the measures of the data logger for each validation set. Two types of climatic data can be used as model inputs: local measurements and satellite data.

Regarding satellite temperature data, the Modern-Era Retrospective analysis for Research and Applications, Version 2 (MERRA-2), provides the ambient temperature with a temporal resolution of 1 minute [47]. Regarding satellite irradiance

data, the Copernicus Atmosphere Monitoring Service provides the direct normal irradiance G_{dn}, the global horizontal one G_{gh} and the diffuse horizontal one G_{dh} for the actual weather conditions with a temporal resolution of 1 minute [48]. It is also possible to use satellite climatic data from other databases such as Meteonorm [49]. The irradiance on the plane of the PV modules G_{pv}, can be deduced from satellite data by [50]:

$$G_{pv}(t) = G_{dn}(t)\cos\big(AOI(t,\theta)\big) + G_{gh}(t)\,\rho\,\frac{1-\cos(\theta)}{2} + G_{dh}(t)\,\frac{1+\cos(\theta)}{2} \tag{10}$$

where ρ is the albedo of the surrounding environment, θ is the tilt of the PV modules, AOI is the angle of incidence between the sun's rays and the PV modules. The AOI is computed by using the MATLAB library PVLIB developed by the Sandia National Laboratories [51].

For the PVWPS of Gogma, according to the observation of the local environment a value of 0.25 is considered for the albedo [42]. We have observed, thanks to simulation, that the influence of the albedo on the irradiance on the plane of the PV modules is very low. This is due to the nearly horizontal position of the PV modules (tilt angle of 0.19 rad i.e. 11°). Figure 10 presents the different components of the irradiance retrieved from the Copernicus Atmosphere Monitoring Service for the location of Gogma and the irradiance on the plane of the PV modules obtained by applying equation (10).

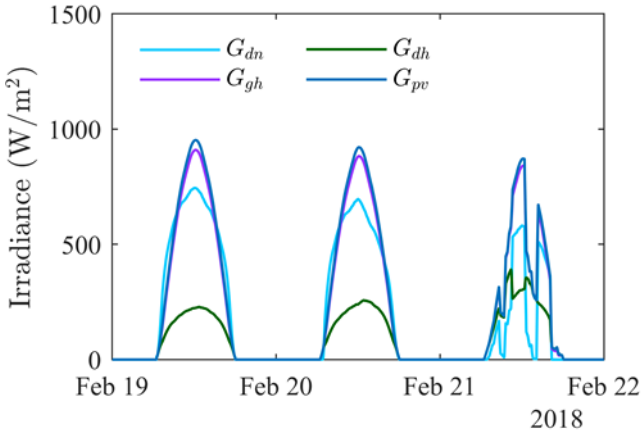

Figure 10 Components of the irradiance from satellite data and derived irradiance on the plane of the PV modules. G_{dn}: direct normal irradiance, G_{gh}: global horizontal irradiance, G_{dh}: diffuse horizontal irradiance, G_{pv}: irradiance on the plane of the PV modules

Figure 11 and Figure 12 present the irradiance on the plane of the PV modules G_{pv} and the ambient temperature T_a obtained from satellite data and from local measurements for the validation set which last from the 19th of February to the 21st of February. Figure 13 shows the collected flow rate Q_c for the same period. G_{pv}, T_a and Q_c are the model inputs. The correlation between local measurements and satellite data is good for irradiance (Figure 11b) and fair for ambient temperature (Figure 12b). However, the latter has a small effect on the model output due to the weak influence of ambient temperature on photovoltaic energy production.

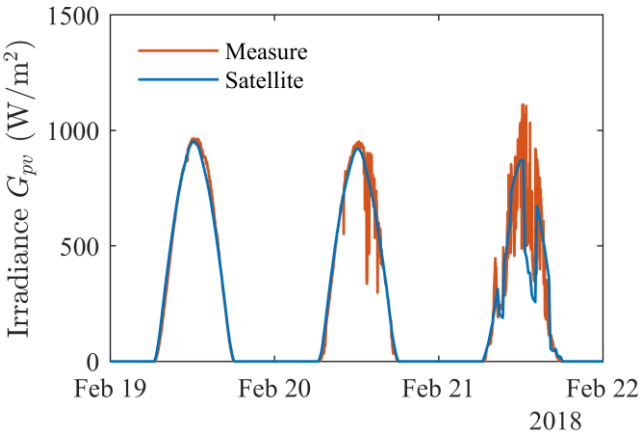

(a)

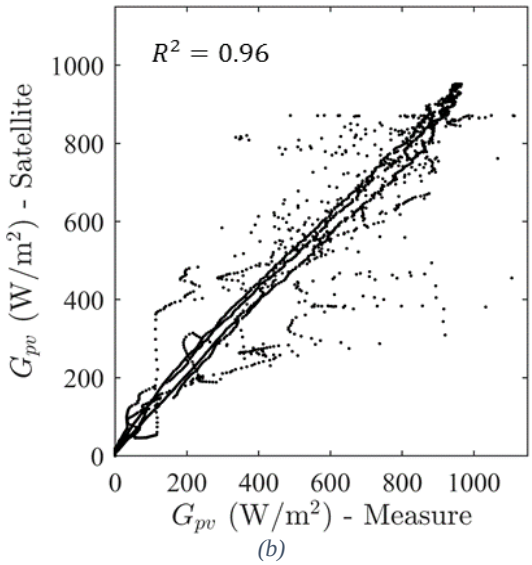

(b)

Figure 11 Irradiance on the plane of the PV modules from satellite data and from local measurements (model input) (a) Temporal evolution (b) scatter plot

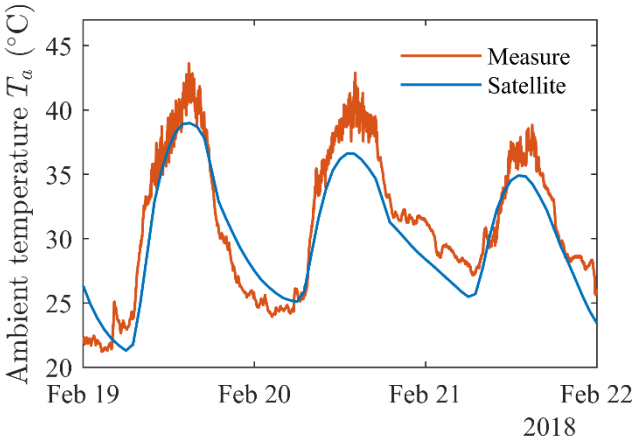

(a)

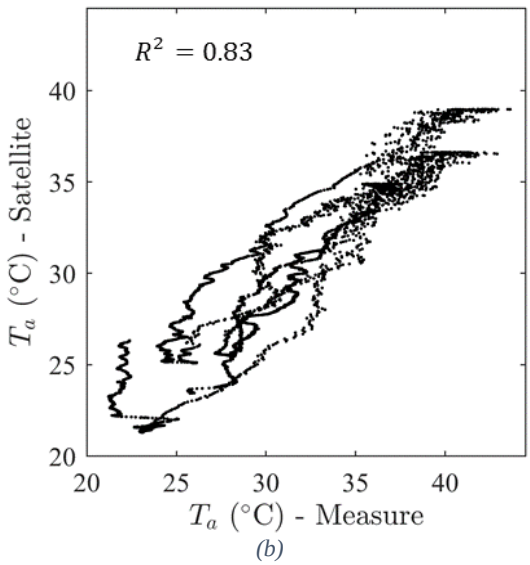

(b)

Figure 12 Ambient temperature from satellite data and from local measurements (model input). (a) Temporal evolution (b) scatter plot

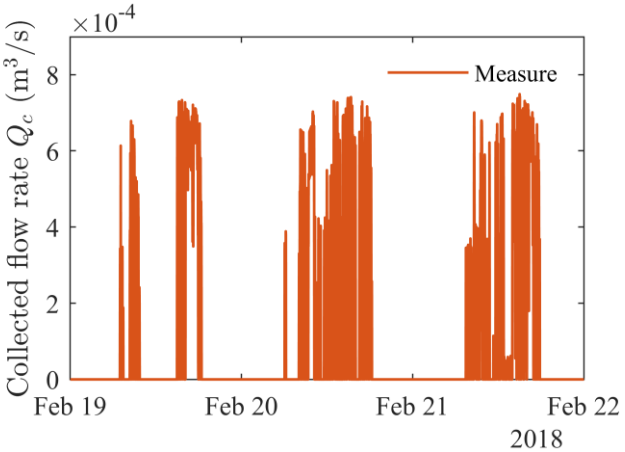

Figure 13 Temporal evolution of the water collection flow rate from local measurements (model input).

The computations for the model for the February validation set start on the 19th of February at 9h20 as the motor-pump has just stopped at this moment and the water height in the tank has just reached the stop level (see section 4.3). Figure 14 compares the measured pumped flow rate Q_p and water height in the tank H_t to the ones obtained from the model with locally measured irradiance and ambient temperature as inputs. Figure 15 does the same comparison but the model inputs are satellite irradiance and satellite ambient temperature.

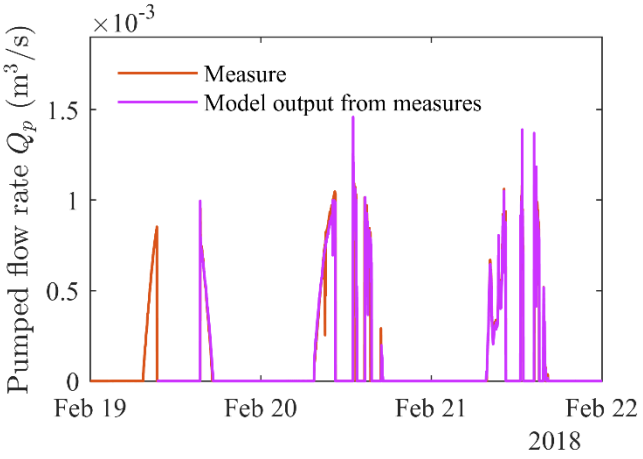

(a)

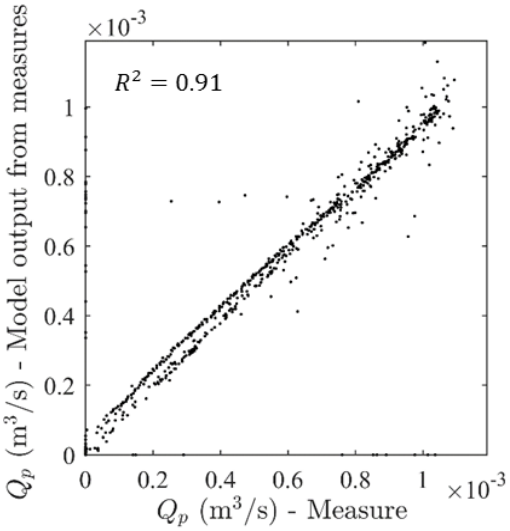

(b)

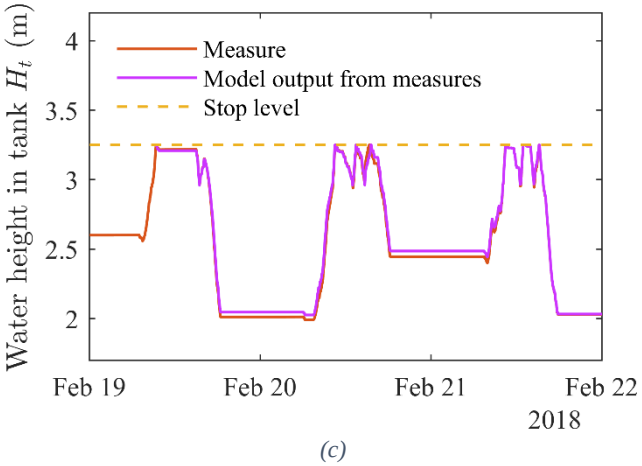

(c)

Figure 14 Pumped flow rate and water height in the tank measured and simulated (model outputs) for local climatic measurements as input.
(a) Pumped flow rate temporal evolution (b) Pumped flow rate scatter plot (c) Water height in the tank temporal evolution

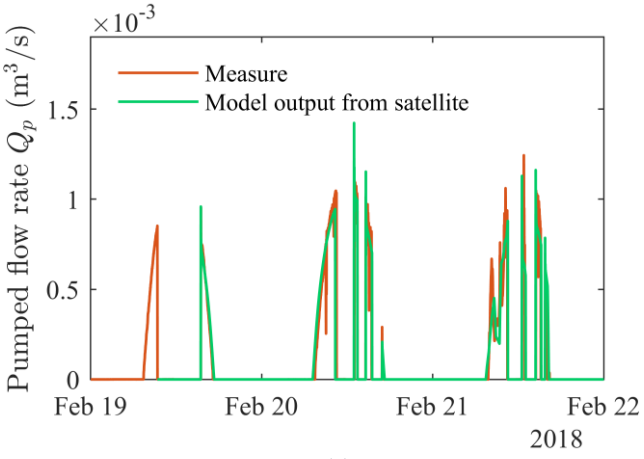

(a)

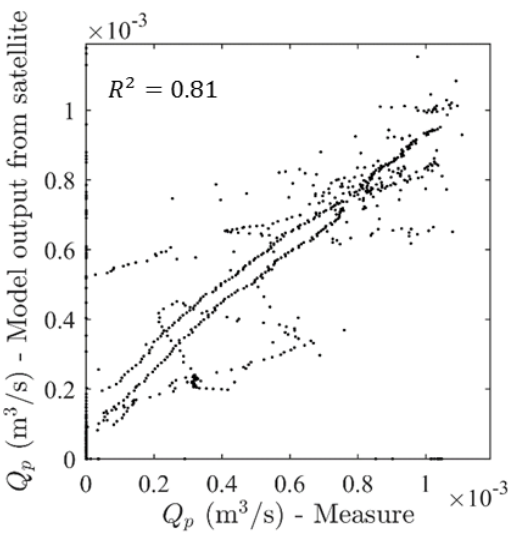

(b)

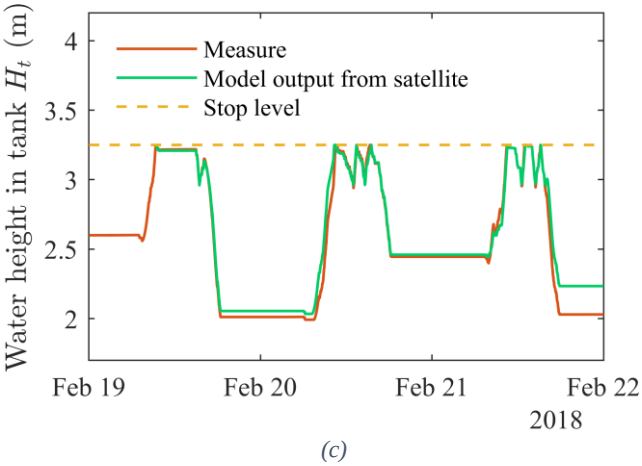

(c)

Figure 15 Pumped flow rate and water height in the tank measured and simulated (model outputs) for satellite climatic data as input.
(a) Pumped flow rate temporal evolution (b) Pumped flow rate scatter plot (c) Water height in the tank temporal evolution

In order to evaluate the performances of the model we study more closely the simulation of the water height in the tank (Figures 14c and 15c). Indeed, it is the most crucial parameter when sizing or analyzing the performances of PVWPS as the water level in the tank must always remain higher than 0 in order to fulfil the water needs of the inhabitants. The root mean square error $RMSE$ between the measured and modelled height in the water tank is of 0.03 m for measured climatic data as model input and of 0.19 m for satellite climatic data as model input. The $RMSE$ values are normalized by the height

between the bottom of the tank and the stop level $H_{t,s}$, which is of 3.3 m, in order to obtain the normalized root mean square errors ($NRMSE$). For the validation period of February, the model allows to predict the water level in the tank with 1.0 % error with measured climatic data as input and with 2.7 % error with satellite climatic data as input.

The same results were computed for the two-week validation sets in May and July-August 2018. The $NRMSE$ for the May period is of 4.8 % when measured climatic data are used as input and of 5.9 % when satellite climatic data are used as input. The $NRMSE$ for the July-August period is 3.8 % with measured climatic data as input and of 5.9 % with satellite climatic data as input. Moreover, for all 3 validation periods and for measured and satellite data as input, the absolute value of the difference between the instantaneous measured and modelled water heights in the tank does not durably increase or decrease along the validation period.

The results indicate that the error for measured data as input is higher for periods which are far from the identification period (May and July-August). This may be due to changes in the parameters of the system such as the static water level in the borehole. Moreover, for the May and July-August periods the errors obtained with satellite and measured data as input are similar. However, it is important to keep in mind that the results with satellite data as input may depend on the location for which satellite data are obtained and on the database from which they are retrieved.

6 Conclusion

The model succeeded in accounting for a previously unaccounted input, i.e., water collection by the users of the PVWPS. The inclusion of the new input allows to model PVWPS with a tank and a control loop on the water level in the tank, which is a common architecture for providing domestic water in off-grid areas of developing countries. We also proposed a methodology for identifying the unknown parameters of the considered PVWPS. Thanks to this methodology, the accuracy of the model is higher than 95 % when using climatic data from local sensors as model input. In addition, we showed that the accuracy drops of only 1 to 3 % when replacing local climatic data by satellite ones. As a consequence, as local climatic measurements may be replaced by satellite data, only the water collection profile would have to be estimated locally to apply the PVWPS model in a given village. This simplifies the simulation of PVWPS performances in other geographic areas. Finally, the parameters of the system in Gogma, Burkina Faso, and the experimental data collected may serve as reference for other installations that aim at communal water access in rural areas of Sub-Saharan Africa.

7 Appendix: Motor-pump model polynomial coefficients

Polynomial	$\boldsymbol{Q_p = P_a^{4,4}(P_{pv}, TDH)}$			$\boldsymbol{TDH = P_b^{4,4}(P_{pv}, Q_p)}$		
Formula	$Q_p = \sum_{m+n=0}^{m+n=4} k_{m,n} {P_{pv}}^m \, TDH^n$			$TDH = \sum_{m+n=0}^{m+n=4} l_{m,n} {P_{pv}}^m \, {Q_p}^n$		
Coefficients	**Index**	**Value**	**Unit**	**Index**	**Value**	**Unit**
	$k_{0,0}$	$2.3\ 10^{-4}$	$m^3\ s^{-1}$	$l_{0,0}$	4.2	m
	$k_{1,0}$	$6.5\ 10^{-6}$	$m^3\ s^{-1}$	$l_{1,0}$	$1.5\ 10^{-1}$	$m\ W^{-1}$
	$k_{0,1}$	$-5.2\ 10^{-5}$	$m^2\ s^{-1}$	$l_{0,1}$	$-3.4\ 10^{4}$	$m^{-2}\ s$
	$k_{2,0}$	$-7.3\ 10^{-9}$	$m^3\ s^{-1}\ W^{-2}$	$l_{2,0}$	$-6.1\ 10^{-5}$	$m\ W^{-2}$
	$k_{1,1}$	$-2.9\ 10^{-8}$	$m^2\ s^{-1}\ W^{-1}$	$l_{1,1}$	$-1.4\ 10^{2}$	$m^{-2}\ s\ W^{-1}$
	$k_{0,2}$	$8.3\ 10^{-8}$	$m\ s^{-1}$	$l_{0,2}$	$5.4\ 10^{7}$	$m^{-5}\ s^2$
	$k_{3,0}$	$3.6\ 10^{-12}$	$m^3\ s^{-1}\ W^{-3}$	$l_{3,0}$	$5.2\ 10^{-8}$	$m\ W^{-3}$
	$k_{2,1}$	$1.1\ 10^{-10}$	$m^2\ s^{-1}\ W^{-2}$	$l_{2,1}$	$-1.5\ 10^{-2}$	$m^{-2}\ s\ W^{-2}$
	$k_{1,2}$	$-2.0\ 10^{-9}$	$m\ s^{-1}\ W^{-1}$	$l_{1,2}$	$9.4\ 10^{4}$	$m^{-5}\ s^2\ W^{-1}$
	$k_{0,3}$	$2.8\ 10^{-8}$	s^{-1}	$l_{0,3}$	$-4.1\ 10^{10}$	$m^{-8}\ s^3$
	$k_{4,0}$	$-6.7\ 10^{-16}$	$m^3\ s^{-1}\ W^{-4}$	$l_{4,0}$	$-2.1\ 10^{-11}$	$m\ W^{-4}$
	$k_{3,1}$	$-3.9\ 10^{-14}$	$m^2\ s^{-1}\ W^{-3}$	$l_{3,1}$	$1.8\ 10^{-5}$	$m^{-2}\ s\ W^{-3}$
	$k_{2,2}$	$1.5\ 10^{-13}$	$m\ s^{-1}\ W^{-2}$	$l_{2,2}$	-15	$m^{-5}\ s^2\ W^{-2}$
	$k_{1,3}$	$1.0\ 10^{-11}$	$s^{-1}\ W^{-1}$	$l_{1,3}$	$-1.3\ 10^{7}$	$m^{-8}\ s^3\ W^{-1}$
	$k_{0,4}$	$-2.6\ 10^{-10}$	$m^{-1}\ s^{-1}$	$l_{0,4}$	$7.8\ 10^{12}$	$m^{-11}\ s^4$

Table 3 Fitting coefficients for the motor-pump model.

8 Acknowledgments

This work is supported by a public grant overseen by the French National research Agency (ANR) as part of the « Investissement d'Avenir » program, through the "IDI 2015" project funded by the IDEX Paris-Saclay, ANR-11-IDEX0003-02. We would like to thank the anonymous reviewers and the editor for their comments and suggestions which allowed to significantly improve the article.

9 References

[1] World Bank, "Access to electricity, rural (% of rural population)," 2016, URL: https://data.worldbank.org/indicator/EG.ELC.ACCS.RU.ZS [accessed 17 December 2018].

[2] United Nations, "The Millennium Development Goals Report," 2015, URL: http://www.un.org/millenniumgoals/2015_MDG_Report/pdf/MDG%202015%20rev%20(July%201).pdf [accessed 10 October 2018].

[3] F. Carlevaro and C. Gonzalez, "Costing Improved Water Supply Systems for Low-income Communities: A Practical Manual", 1st ed., IWA Publishing, 2015.

[4] J. Bartram and S. Cairncross, "Hygiene, Sanitation, and Water: Forgotten Foundations of Health," PLoS Med., vol. 7, no. 11, p. e1000367, Nov. 2010, DOI: 10.1371/journal.pmed.1000367.

[5] Agence Française de Développement and Programme Solidarité Eau, "Réalisation et gestion des forages équipés d'une pompe à motricité humaine en Afrique subsaharienne," 2011, URL : https://www.pseau.org/outils/ouvrages/afd_realisation_et_gestion_des_forages_equipes_d_une_pompe_a_motricite_humaine_en_afrique_subsaharienne_2011.pdf [accessed 10 October 2018].

[6] H.C. Bonsor, A.M. Macdonald, "An initial estimate of depth to groundwater across Africa", British Geological Survey Open Report, URL: http://nora.nerc.ac.uk/id/eprint/17907/1/OR11067.pdf [accessed 17 December 2018].

[7] Fraunhofer ISE, "Current and Future Cost of Photovoltaics. Long-term Scenarios for Market Development, System Prices and LCOE of Utility-Scale PV Systems," Study on behalf of Agora Energiewende, 2015, URL: https://www.ise.fraunhofer.de/content/dam/ise/de/documents/publications/studies/AgoraEnergiewende_Current_and_Future_Cost_of_PV_Feb2015_web.pdf [accessed 10 October 2018]

[8] S. S. Chandel, M. Nagaraju Naik, and R. Chandel, "Review of solar photovoltaic water pumping system technology for irrigation and community drinking water supplies," Renew. Sustain. Energy Rev., vol. 49, pp. 1084–1099, Sep. 2015, DOI: 10.1016/j.rser.2015.04.083.

[9] S. Ould-Amrouche, D. Rekioua, and A. Hamidat, "Modelling photovoltaic water pumping systems and evaluation of their CO2 emissions mitigation potential," Appl. Energy, vol. 87, no. 11, pp. 3451–3459, Nov. 2010, DOI: 10.1016/j.apenergy.2010.05.021.

[10] A. M. Armanuos, A. Negm, and A. H. M. H. El Tahan, "Life Cycle Assessment of Diesel Fuel and Solar Pumps in Operation Stage for Rice Cultivation in Tanta, Nile Delta, Egypt," Procedia Technol., vol. 22, pp. 478–485, 2016, DOI: 10.1016/j.protcy.2016.01.095.

[11] J. V. Mapurunga Caracas, G. De Carvalho Farias, L. F. Moreira Teixeira, and L. A. De Souza Ribeiro, "Implementation of a High-Efficiency, High-Lifetime, and Low-Cost Converter for an Autonomous Photovoltaic Water Pumping System," IEEE Trans. Ind. Appl., vol. 50, no. 1, pp. 631–641, Jan. 2014, DOI: 10.1109/TIA.2013.2271214.

[12] M. I. Chergui and M. O. Benaissa, "Strategy photovoltaic pumping system in scattered area," International Conference on Renewable Energy Research and Applications (ICRERA), Palermo, pp. 283–286, Nov. 2015, DOI: 10.1109/ICRERA.2015.7418710.

[13] P. E. Campana, H. Li, and J. Yan, "Dynamic modelling of a PV pumping system with special consideration on water demand," Appl. Energy, vol. 112, pp. 635–645, Dec. 2013, DOI: 10.1016/j.apenergy.2012.12.073.

[14] A. Hamidat and B. Benyoucef, "Mathematic models of photovoltaic motor-pump systems," Renew. Energy, vol. 33, no. 5, pp. 933–942, May 2008, DOI: 10.1016/j.renene.2007.06.023.

[15] A. Djoudi Gherbi, A. Hadj Arab, and H. Salhi, "Improvement and validation of PV motor-pump model for PV pumping system performance analysis," Sol. Energy, vol. 144, pp. 310–320, Mar. 2017, DOI: 10.1016/j.solener.2016.12.042.

[16] J. K. Kaldellis, E. Meidanis, and D. Zafirakis, "Experimental energy analysis of a stand-alone photovoltaic-based water pumping installation," Appl. Energy, vol. 88, no. 12, pp. 4556–4562, Dec. 2011, DOI: 10.1016/j.apenergy.2011.05.036

[17] S. Sallem, M. Chaabene, and M. B. A. Kamoun, "Energy management algorithm for an optimum control of a photovoltaic water pumping system," Appl. Energy, vol. 86, no. 12, pp. 2671–2680, Dec. 2009, DOI: 10.1016/j.apenergy.2009.04.018

[18] A. K. Tiwari and V. R. Kalamkar, "Effects of total head and solar radiation on the performance of solar water pumping system," Renew. Energy, vol. 118, pp. 919–927, Apr. 2018, DOI: 10.1016/j.renene.2017.11.004

[19] K. Yadav, A. Kumar, O. S. Sastry, and R. Wandhare, "Solar photovoltaics pumps operating head selection for the optimum efficiency," Renew. Energy, vol. 134, pp. 169–177, Apr. 2019, online Nov. 2018, DOI: 10.1016/j.renene.2018.11.013

[20] P. E. Campana, H. Li, J. Zhang, R. Zhang, J. Liu, and J. Yan, "Economic optimization of photovoltaic water pumping systems for irrigation," Energy Convers. Manag., vol. 95, pp. 32–41, May 2015, DOI: 10.1016/j.enconman.2015.01.066.

[21] J. Zhang, J. Liu, P. E. Campana, R. Zhang, J. Yan, and X. Gao, "Model of evapotranspiration and groundwater level based on photovoltaic water pumping system," Appl. Energy, vol. 136, pp. 1132–1137, Dec. 2014, DOI: 10.1016/j.apenergy.2014.05.045.

[22] E. H. Amer and M. A. Younes, "Estimating the monthly discharge of a photovoltaic water pumping system: Model verification," Energy Convers. Manag., vol. 47, no. 15–16, pp. 2092–2102, Sep. 2006, DOI: 10.1016/j.enconman.2005.12.001.

[23] S. Haddad, M. Benghanem, A. Mellit, and K. O. Daffallah, "ANNs-based modeling and prediction of hourly flow rate of a photovoltaic water pumping system: Experimental validation," Renew. Sustain. Energy Rev., vol. 43, pp. 635–643, Mar. 2015, DOI: 10.1016/j.rser.2014.11.083.

[24] M. Benghanem, K. O. Daffallah, and A. Almohammedi, "Estimation of daily flow rate of photovoltaic water pumping systems using solar radiation data," Results Phys., vol. 8, pp. 949–954, Mar. 2018, DOI: 10.1016/j.rinp.2018.01.022

[25] A. A. Peralta Vera, H. J. del Carpio Beltrán, J. C. Zuñiga Torres, J. J. Milón Guzmán, and S. L. Braga, "Experimental study of a photovoltaic DC water pumping system for irrigation in rural-isolated region of Arequipa, Peru," J. Sol. Energy Eng., vol. 141, no. 4, Feb. 2019, DOI: 10.1115/1.4042724.

[26] U. Deichmann, C. Meisner, S. Murray, and D. Wheeler, "The economics of renewable energy expansion in rural Sub-Saharan Africa," Energy Policy, vol. 39, no. 1, pp. 215–227, Jan. 2011, DOI: 10.1016/j.enpol.2010.09.034.

[27] A. Hamidat and B. Benyoucef, "Systematic procedures for sizing photovoltaic pumping system, using water tank storage," Energy Policy, vol. 37, no. 4, pp. 1489–1501, Apr. 2009, DOI: 10.1016/j.enpol.2008.12.014.

[28] B. Bouzidi, M. Haddadi, and O. Belmokhtar, "Assessment of a photovoltaic pumping system in the areas of the Algerian Sahara," Renew. Sustain. Energy Rev., vol. 13, no. 4, pp. 879–886, May 2009, DOI: 10.1016/j.rser.2008.01.013.

[29] A. Hamidat, B. Benyoucef, and T. Hartani, "Small-scale irrigation with photovoltaic water pumping system in Sahara regions," Renew. Energy, vol. 28, no. 7, pp. 1081–1096, 2003, DOI: 10.1016/S0960-1481(02)00058-7.

[30] I. Yahyaoui, A. Atieh, A. Serna, and F. Tadeo, "Sensitivity analysis for photovoltaic water pumping systems: Energetic and economic studies," Energy Convers. Manag., vol. 135, pp. 402–415, Mar. 2017, DOI: 10.1016/j.enconman.2016.12.096.

[31] D. H. Muhsen, A. B. Ghazali, T. Khatib, I. A. Abed, and E. M. Natsheh, "Sizing of a standalone photovoltaic water pumping system using a multi-objective evolutionary algorithm," Energy, vol. 109, pp. 961–973, Aug. 2016, DOI: 10.1016/j.energy.2016.05.070.

[32] A. A. Ghoneim, "Design optimization of photovoltaic powered water pumping systems," Energy Convers. Manag., vol. 47, no. 11–12, pp. 1449–1463, Jul. 2006, DOI: 10.1016/j.enconman.2005.08.015.

[33] J. K. Kaldellis, G. C. Spyropoulos, K. A. Kavadias, and I. P. Koronaki, "Experimental validation of autonomous PV-based water pumping system optimum sizing," Renew. Energy, vol. 34, no. 4, pp. 1106–1113, Apr. 2009, DOI: 10.1016/j.renene.2008.06.021.

[34] Z. Girma, "Techno-economic analysis of photovoltaic pumping system for rural water supply in Ethiopia," Int. J. Sustain. Energy, vol. 36, no. 3, pp. 277–295, Mar. 2017, DOI: 10.1080/14786451.2015.1017498.

[35] P. E. Campana, H. Li, and J. Yan, "Techno-economic feasibility of the irrigation system for the grassland and farmland conservation in China: Photovoltaic vs. wind power water pumping," Energy Convers. Manag., vol. 103, pp. 311–320, Oct. 2015, DOI: 10.1016/j.enconman.2015.06.034.

[36] C. Zhang, P. E. Campana, J. Yang, C. Yu, and J. Yan, "Economic assessment of photovoltaic water pumping integration with dairy milk production," Energy Convers. Manag., vol. 177, pp. 750–764, Dec. 2018, DOI: 10.1016/j.enconman.2018.09.060.

[37] A. Allouhi, M. S. Buker, H. El-houari, A. Boharb, M. Benzakour Amine, T. Kousksou, A. Jamil, "PV water pumping systems for domestic uses in remote areas: Sizing process, simulation and economic evaluation," Renew. Energy, vol. 132, pp. 798–812, Mar. 2019, online Aug. 2018, DOI: 10.1016/j.renene.2018.08.019.

[38] Grundfos, "Performance curve of SQFlex 5A-7 motor-pump," URL: https://product-selection.grundfos.com/product-detail.product-detail.html?custid=GMA&productnumber=95027342&qcid=421916400 [accessed 05 October 2018].

[39] Grundfos, "CU 200 controller," URL: https://product-selection.grundfos.com/product-detail.product-detail.html?custid=GMA&productnumber=96625360 [accessed 05 October 2018].

[40] M. Koehl, M. Heck, S. Wiesmeier, and J. Wirth, "Modeling of the nominal operating cell temperature based on outdoor weathering," Sol. Energy Mater. Sol. Cells, vol. 95, no. 7, pp. 1638–1646, Jul. 2011, 10.1016/j.solmat.2011.01.020.

[41] S. Ponce-Alcántara, J. P. Connolly, G. Sánchez, J. M. Míguez, V. Hoffmann, and R. Ordás, "A Statistical Analysis of the Temperature Coefficients of Industrial Silicon Solar Cells," Energy Procedia, vol. 55, pp. 578–588, 2014, DOI: 10.1016/j.egypro.2014.08.029.

[42] A. McEvoy, T. Markvart, and L. Castañer, Practical Handbook of Photovoltaics - Fundamental and Applications, 2nd ed., Academic Press, 2011.

[43] Fraunhofer ISE, "Photovoltaics report," Feb. 2018, URL: https://www.ise.fraunhofer.de/content/dam/ise/de/documents/publications/studies/Photovoltaics-Report.pdf [accessed 10 October 2018].

[44] W. H. Bierschenk, "Determining well efficiency by multiple step-drawdown tests," International Association of Scientific Hydrology, 1963, URL: http://hydrologie.org/redbooks/a064/064043.pdf [accessed 05 October 2018].

[45] T. E. Reilly, L. Franke, and G. D. Bennett, "The principle of superposition and its application in ground-water hydraulics," US Geol. Surv., Open-File Report 84-459, 1987, URL: https://pubs.usgs.gov/of/1984/0459/report.pdf [accessed 05 October 2018].

[46] B. R. Munson, D. F. Young, and T. H. Okiishi, Fundamentals of Fluid Mechanics, 5th ed., Wiley, 2006.

[47] NASA, "Modern-Era Retrospective analysis for Research and Applications, Version 2," 2017, URL: https://gmao.gsfc.nasa.gov/reanalysis/MERRA-2/ [accessed 01 October 2018].

[48] European Commission, "Copernicus Atmosphere Monitoring Service (CAMS)," 2017, URL: http://www.soda-pro.com/web-services/radiation/cams-radiation-service [accessed 01 October 2018].

[49] Meteonorm, 2018, URL: https://meteonorm.com/en/ [accessed 17 December 2018].

[50] L. Fraas and L. Partain, Solar cells and their applications, 2nd ed., Wiley, 2010.

[51] Sandia National Laboratories,"PV_LIB Toolbox", 2018, URL: https://pvpmc.sandia.gov/applications/pv_lib-toolbox/ [accessed 02 December 2018].